Important Notice to Authors

No further publication processing will occur until we receive your response to this proof.

Attached is a PDF proof of your forthcoming article in *Physical Review X*. The article accession code is XB10482.

Your paper has been assigned the following Subject Area labels: Condensed Matter Physics, Spintronics, Topological Insulators

Your paper will be in the following section of the journal: RESEARCH ARTICLES

Please note that as part of the production process, APS converts all articles, regardless of their original source, into standardized XML that in turn is used to create the PDF and online versions of the article as well as to populate third-party systems such as Portico, Crossref, and Web of Science. We share our authors' high expectations for the fidelity of the conversion into XML and for the accuracy and appearance of the final, formatted PDF. This process works exceptionally well for the vast majority of articles; however, please check carefully all key elements of your PDF proof, particularly any equations or tables.

Figures submitted electronically as separate files containing color appear in color in the journal.

Specific Questions and Comments to Address for This Paper

The numbered items below correspond to numbers in the margin of the proof pages pinpointing the source of the question and/or comment. The numbers will be removed from the margins prior to publication.

1 Second proof: Please carefully confirm that all first-proof corrections were addressed and that changes were made accurately.

2 Second proof: Please note that there is no "Topological Materials" subject area in subject area database. Hence, the requested correction could not be made.

3 Second proof: Please check and approve that the paper is ready to be published in its current form.

ORCIDs

Please follow any ORCID links (iD) after the authors' names and verify that they point to the appropriate record for each author.

Funding Information

Information about an article's funding sources is now submitted to Crossref to help you comply with current or future funding agency mandates. Crossref's Open Funder Registry (https://www.crossref.org/services/funder-registry/) is the definitive registry of funding agencies. Please ensure that your acknowledgments include all sources of funding for your article following any requirements of your funding sources. Where possible, please include grant and award ids. Please carefully check the following funder information we have already extracted from your article and ensure its accuracy and completeness:

- National Science Foundation, FundRef ID http://dx.doi.org/10.13039/100000001 (US/United States)
- Welch Foundation, FundRef ID http://dx.doi.org/10.13039/100000928 (US/United States)
- National Research Foundation of Korea, FundRef ID http://dx.doi.org/10.13039/501100003725 (KR/Republic of Korea)
- University of Edinburgh, FundRef ID http://dx.doi.org/10.13039/501100000848 (GB/United Kingdom of Great Britain and Northern Ireland)

- Engineering and Physical Sciences Research Council, FundRef ID http://dx.doi.org/10.13039/501100000266 (GB/United Kingdom of Great Britain and Northern Ireland)
- ARCHER Service, FundRef ID http://dx.doi.org/10.13039/501100016989 (GB/United Kingdom of Great Britain and Northern Ireland)
- U.S. Department of Energy, FundRef ID http://dx.doi.org/10.13039/100000015 (US/United States)
- Oak Ridge National Laboratory, FundRef ID http://dx.doi.org/10.13039/100006228 (US/United States)

Other Items to Check

- Please note that the original manuscript has been converted to XML prior to the creation of the PDF proof, as described above. Please carefully check all key elements of the paper, particularly the equations and tabular data.
- Please ignore the text of the Popular Summary, it is not the final version. An APS science writer will work with you separately to edit the summary.
- Title: Please check; be mindful that the title may have been changed during the peer-review process.
- Author list: Please make sure all authors are presented, in the appropriate order, and that all names are spelled correctly.
- Please make sure you have inserted a byline footnote containing the email address for the corresponding author, if desired. Please note that this is not inserted automatically by this journal.
- Affiliations: Please check to be sure the institution names are spelled correctly and attributed to the appropriate author(s).
- Receipt date: Please confirm accuracy.
- Acknowledgments: Please be sure to appropriately acknowledge all funding sources.
- Hyphenation: Please note hyphens may have been inserted in word pairs that function as adjectives when they occur before a noun, as in “x-ray diffraction,” “4-mm-long gas cell,” and “*R*-matrix theory.” However, hyphens are deleted from word pairs when they are not used as adjectives before nouns, as in “emission by x rays,” “was 4 mm in length,” and “the *R* matrix is tested.”
  Note also that Physical Review follows U.S. English guidelines in that hyphens are not used after prefixes or before suffixes: superresolution, quasiequilibrium, nanoprecipitates, resonancelike, clockwise.
- Please check that your figures are accurate and sized properly. Make sure all labeling is sufficiently legible. Figure quality in this proof is representative of the quality to be used in the online journal. To achieve manageable file size for online delivery, some compression and downsampling of figures may have occurred. Fine details may have become somewhat fuzzy, especially in color figures. Figures to be published in color online will appear in color on these proofs if viewed on a color monitor or printed on a color printer.
- Overall, please proofread the entire *formatted* article very carefully. The redlined PDF should be used as a guide to see changes that were made during copyediting. However, note that some changes to math and/or layout may not be indicated.

Ways to Respond

- ***Web:*** If you accessed this proof online, follow the instructions on the web page to submit corrections.
- ***Email:*** Send corrections to aps-robot@luminad.com. Include the accession code XB10482 in the subject line.
- ***Fax:*** Return this proof with corrections to +1.855.808.3897.

If You Need to Call Us

You may leave a voicemail message at +1.855.808.3897. Please reference the accession code and the first author of your article in your voicemail message. We will respond to you via email.

Popular Summary

A van der Waals material is made of a stack of weakly bonded planes of atoms. These 2D materials are powerful platforms for exploring several electronic and magnetic behaviors. Recently, the discovery of robust topological spin excitations in the 2D magnet CrI_3 has spurred huge interest in their potential applications such as in the field of dissipationless spintronics, where electron spins are used to transmit and store information. Here, we use neutron-scattering experiments to explore the microscopic origin of these spin excitations and an accompanying intriguing magnetic phenomenon in this material: a stacking-dependent magnetic order. That is, while a single layer of CrI_3 is ferromagnetic, two stacked layers are antiferromagnetic, which, counterintuitively, is different from that in the ferromagnetic bulk.

In our experiments, we find that spin-orbit coupling (a relativistic interaction of an electron's spin with its motion) induces asymmetric interactions between the spins. This induces the spins to feel the magnetic field differently, affecting their topological excitations. In addition, our measurements show that the nearest magnetic exchange interaction along the weakly bonded planes is indeed antiferromagnetic.

Our results unveil the origin of the observed antiferromagnetic order in thin layers of CrI_3 and provide a new understanding of topology-driven spin excitations in 2D van der Waals magnets.

Magnetic Field Effect on Topological Spin Excitations in CrI_3

Lebing Chen,[1] Jae-Ho Chung,[2,*] Matthew B. Stone,[3] Alexander I. Kolesnikov,[3] Barry Winn,[3] V. Ovidiu Garlea,[3] Douglas L. Abernathy,[3] Bin Gao,[1] Mathias Augustin,[4] Elton J. G. Santos,[4,5,†] and Pengcheng Dai[1,‡]
[1]Department of Physics and Astronomy, Rice University, Houston, Texas 77005, USA
[2]Department of Physics, Korea University, Seoul 02841, Korea
[3]Neutron Scattering Division, Oak Ridge National Laboratory, Oak Ridge, Tennessee 37831, USA
[4]Institute for Condensed Matter Physics and Complex Systems, School of Physics and Astronomy, The University of Edinburgh, EH9 3FD, United Kingdom
[5]Higgs Centre for Theoretical Physics, The University of Edinburgh, EH9 3FD, United Kingdom

(Received 18 February 2021; revised 6 May 2021; accepted 10 June 2021)

The search for topological spin excitations in recently discovered two-dimensional (2D) van der Waals (vdW) magnetic materials is important because of their potential applications in dissipationless spintronics. In the 2D vdW ferromagnetic (FM) honeycomb lattice CrI_3 ($T_C = 61$ K), acoustic and optical spin waves are found to be separated by a gap at the Dirac points. The presence of such a gap is a signature of topological spin excitations if it arises from the next-nearest-neighbor (NNN) Dzyaloshinskii-Moriya (DM) or bond-angle-dependent Kitaev interactions within the Cr honeycomb lattice. Alternatively, the gap is suggested to arise from an electron correlation effect not associated with topological spin excitations. Here, we use inelastic neutron scattering to conclusively demonstrate that the Kitaev interactions and electron correlation effects cannot describe spin waves, Dirac gaps, and their in-plane magnetic field dependence. Our results support the idea that the DM interactions are the microscopic origin of the observed Dirac gap. Moreover, we find that the nearest-neighbor (NN) magnetic exchange interactions along the c axis are antiferromagnetic (AF), and the NNN interactions are FM. Therefore, our results unveil the origin of the observed c-axis AF order in thin layers of CrI_3, firmly determine the microscopic spin interactions in bulk CrI_3, and provide a new understanding of topology-driven spin excitations in 2D vdW magnets.

DOI: Subject Areas: Condensed Matter Physics, Spintronics, Topological Insulators

I. INTRODUCTION

The discovery of robust two-dimensional (2D) ferromagnetic (FM) long-range order in monolayer van der Waals (vdW) magnets [1–3] is important because these materials can provide a new platform to study fundamental physics without the influence of a substrate and can potentially be used to develop new spintronic devices [4,5]. One prominent group of these materials includes the chromium trihalides, CrX_3 (X = Br, I) or $CrXTe_3$ (X = Ge, Si), where Cr^{3+} ($3d^3$, $S = 3/2$) ions form 2D honeycomb lattices [Fig. 1(a)] [6,7]. Within a single honeycomb layer, Cr^{3+} ions interact with each other ferromagnetically via the nearly 90-degree Cr-X-Cr superexchange paths [Fig. 1(b)] [8]. Although the $3d$ electrons of Cr^{3+} do not provide large spin-orbit coupling (SOC), the heavier ligand atoms such as iodine may serve as a source of significant SOC. This not only provides the thermal stability observed in vdW layered materials but also enriches the physics of magnetism in the 2D limit [9–14]. Indeed, it is proposed that the Kitaev interaction [15], known to be important for effective $S = 1/2$ honeycomb lattice magnets near a Kitaev quantum spin liquid [16,17], may occur in $S = 3/2$ CrI_3 across the nearest bond with bond-dependent anisotropic Ising-like exchange [Fig. 1(b)]. This occurrence would be critical for the magnetic stability of monolayer CrI_3 and spin dynamics in bulk CrI_3 [18–22]. Furthermore, spin waves (magnons) from honeycomb ferromagnets can be topological by opening a gap at the Dirac points via time-reversal symmetry breaking (TRSB) [23,24]. As a magnetic analog of electronic dispersion in graphene [25], spin-wave spectra of honeycomb ferromagnets have Dirac points at the Brillouin zone boundaries where dispersions of acoustic and optical spin waves meet and produce Dirac cones. If the system has TRSB arising from a large SOC, one would expect to observe an energy gap at the Dirac point of the bulk magnon bands [23], analogous to

*jaehc@korea.ac.kr
†esantos@exseed.ed.ac.uk
‡pdai@rice.edu

the SOC-induced gap at the Dirac point in the electronic dispersion of graphene [26]. This energy gap, in turn, would allow the realization of massless topological spin excitations propagating without dissipation [27–29].

Experimentally, a spin gap was indeed observed at the Dirac point in the spin-wave spectra of the honeycomb lattice FM CrI_3 [30]. Three possible scenarios have been proposed to understand the observed spin gap. The first corresponds to the Dzyaloshinskii-Moriya (DM) interaction that occurs on the bonds without inversion symmetry [Figs. 1(a), 1(c), and 1(d)] [31,32]. The second scenario is the Kitaev interaction that also breaks time-reversal symmetry and can inhabit nontrivial topological edge modes [19,33]. Finally, the observed Dirac spin gap is suggested to arise from electron correlations that must be treated explicitly to understand the spin dynamics in CrI_3 and the broad family of 2D vdW magnetic materials [34]. In this case, spin excitations in CrI_3 would not be topological.

Another intriguing property of CrI_3 is its weak structural and magnetic coupling along the c axis. In the low-temperature FM phase, bulk CrI_3 is assumed to have rhombohedral lattice structure with space group $R\bar{3}$ [6]. On warming across T_C, the FM order in CrI_3 disappears in a weakly first-order phase transition coupled with a small c-axis lattice parameter change. Upon further warming to 90–200 K, CrI_3 undergoes a first-order phase transition from rhombohedral to monoclinic structure with a $C/2m$ space group, basically shifting the stacking of the CrI_3 layers [6]. From comparisons to spin-wave dispersions, the nearest-neighbor (NN) c axis magnetic exchange coupling is deduced to be FM with $J_{c1} \approx 0.59$ meV [Fig. 1(a)] [30]. However, transport, Raman scattering, scanning magnetic circular dichroism microscopy, and tunneling measurements as a function of film thickness [1,35,36], pressure [37,38], and applied magnetic field [39] suggest A-type antiferromagnetic (AF) structure associated with the monoclinic structure present in the bilayer and a few top layers of bulk CrI_3. In particular, a magnetic field a few Tesla along the c axis was found to modify the crystal lattice symmetry of CrI_3, thus suggesting a strong spin-lattice coupling [39]. Therefore, it is important to determine if the NN interlayer exchange coupling is indeed FM and what determines the overall FM interlayer coupling in the CrI_3 bulk with rhombohedral lattice structure.

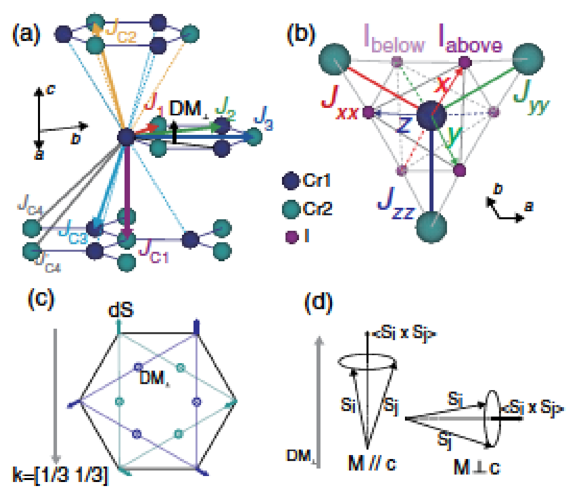

FIG. 1. Crystal structure of CrI_3. (a) CrI_3 rhombohedral lattice showing only Cr atoms, with Cr^{3+} spins along the c axis. Cr1 (blue) and Cr2 (cyan) spheres indicate Cr atoms in different triangular sublattices. The colored bonds indicate in-plane and interlayer magnetic exchange interactions. The cyan and yellow dashed lines show the three J_{c2}'s and six J_{c3}'s around one Cr atom. (b) Kitaev interaction in the local coordinates of CrI_3. The J_{xx}, J_{yy}, J_{zz} bond is between the NNs, and the $\{x, y, z\}$ direction is parallel to the Cr-I bond, as shown with arrows. (c) DM interactions in CrI_3 with a top view of the Cr^{3+} hexagon at the Dirac wave vector. The cyan and blue colors distinguish two triangular sublattices. (d) Interactions between DM and spins. Only when spins have components along the c axis can the DM term give a nonzero contribution to the total Hamiltonian.

In this work, we use high-resolution inelastic neutron scattering to study spin waves of CrI_3 and their magnetic field dependence. By reducing the mosaic of coaligned single crystals of CrI_3 from earlier work [30], we were able to precisely measure the magnitude of the spin gap at the Dirac points and the entire spin-wave spectra. In addition, we determine the effect of an in-plane magnetic field on spin waves and the Dirac spin gap in CrI_3. By comparing the experimental observations with expectations from the Heisenberg-DM and Heisenberg-Kitaev Hamiltonian, and the effect of electron correlations, we conclude that spin waves and the Dirac spin gap in CrI_3 cannot be described by the Heisenberg-Kitaev Hamiltonian and electron correlation effects. Instead, the data are approximately consistent with the Heisenberg-DM Hamiltonian, considering both the c-axis and in-plane DM interactions. Our results therefore clarify the microscopic spin interactions in CrI_3 and provide a new understanding of topology-driven spin excitations in 2D vdW magnets.

II. RESULTS

Single crystalline CrI_3 samples were grown using the chemical-vapor-transport method as described in Ref. [6]. Our inelastic neutron scattering experiments were carried out on either fully coaligned (~0.42 g) or c-axis aligned (~1 g) crystals on the SEQUOIA [40], HYSPEC [41], and ARCS [42] spectrometers at Spallation Neutron Source, Oak Ridge National Laboratory. Consistent with Ref. [30], we use a honeycomb lattice with an in-plane Cr-Cr distance of about 3.96 Å and c-axis layer spacing of 6.62 Å in the low-temperature rhombohedral structure to describe CrI_3. The momentum transfer $\mathbf{Q} = H\mathbf{a}^* + K\mathbf{b}^* + L\mathbf{c}^*$ is denoted as (H, K, L) in reciprocal lattice units (r.l.u.) with marked high-symmetry points [Figs. 2(a) and 2(b)]. All measurements were carried out with the c axis of the sample in the horizontal scattering plane and with the

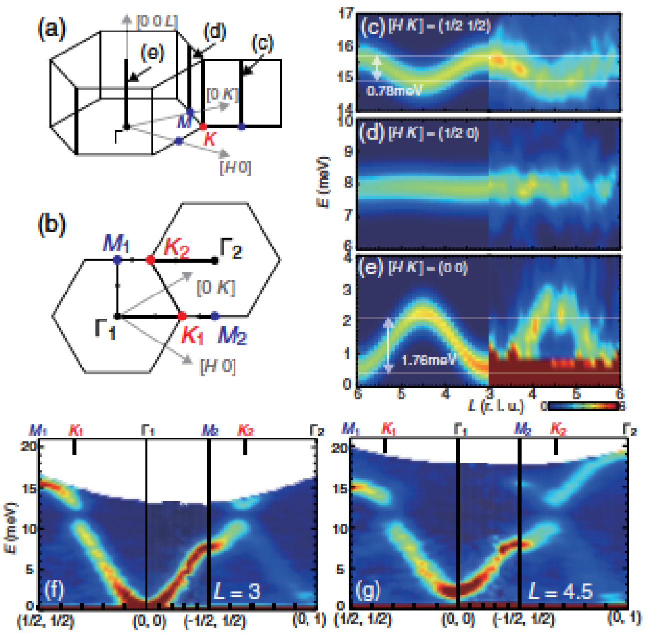

FIG. 2. Spin wave spectra of CrI_3. (a) The hexagonal reciprocal lattice of CrI_3. Gray arrows show reciprocal lattice vectors, and high-symmetry (Γ, K, M) points are specified in blue (M), red (K), and black (Γ) dots, respectively. The bold black lines specify the scan direction in (c–e). (b) Projection of the hexagonal reciprocal lattice in the $[H, K]$ plane. The arrows indicate the scan path of the spectra shown in (f, g), Figs. 3(a)–3(c), and Figs. 4(a) and 4(b). (c–e) The spin wave dispersion along the L direction at different $[H, K]$ positions specified in (a), showing different bandwidths at different $[H, K]$ points. The left and right panels are calculation and data, respectively. (f, g) Spin wave dispersion at different L points. (f) shows L integration range $[2.5, 3.5]$ near the $[0, 0, L]$ band bottom, while (g) shows L integration range $[4, 5]$ near the band top.

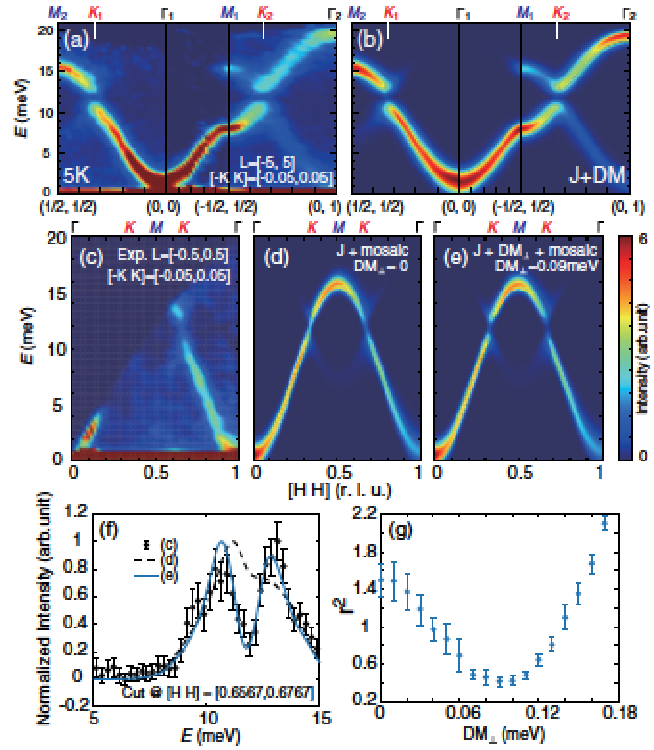

FIG. 3. The Heisenberg-DM model fit of CrI_3 E-$\mathbf{Q}$ spin wave spectrum. High-symmetry points are labeled. (a) Experimental data at 5 K. (b) Heisenberg-DM model simulation using parameters in Table I. (c) Experimental data at 5 K with smaller L integration range. (d, e) Heisenberg-DM model simulations including sample mosaic with (d) $\mathrm{DM} = 0$ and (e) $\mathrm{DM}_\perp = 0.09$ meV. (f) Constant-$\mathbf{Q}$ cuts of the data in (c–e) at the Dirac point $(2/3, 2/3, 0)$. (g) The squared error r^2 between experimental and simulation values of the Dirac point cut as a function of the DM interaction strength.

applied magnetic fields vertical, i.e., in the ab plane of CrI_3 [Figs. 1(a), (c), and (d)].

We begin by describing the zero field high-resolution spin-wave data of CrI_3 obtained on SEQUIOA (Figs. 2 and 3). Figure 3(a) shows the energy-momentum (E-$\mathbf{Q}$)-dependent spin-wave spectra along the high-symmetry directions in reciprocal space as depicted in Fig. 2(a). These in-plane spin-wave spectra were obtained by integrating dispersive spin waves along the c axis over $-5 \leq L \leq 5$. The overall momentum dependence of the spin-wave energies is consistent with previous work [30], revealing two spin-wave modes characteristic of the honeycomb ferromagnets. The lower and upper modes account for the acoustic and optical vibrations, respectively, of the two sublattice spins. These two spin-wave modes will meet each other at the Dirac wave vectors of $Q_{K_1} = (\frac{1}{3}, \frac{1}{3})$ and $Q_{K_2} = (\frac{2}{3}, -\frac{1}{3})$ [Figs. 3(a) and 3(d)]. Inspection of Fig. 3(a) reveals clear evidence of a spin gap of about 2.8 meV, which is approximately 50% the value estimated from previous low-resolution data [30]. This result is mostly due to the reduced mosaicity of the coaligned single crystals (an in-plane mosaic full width at half maximum of 8.0° compared with that of about 17° in Ref. [30]) and improved instrumental resolution [43].

To completely determine the spin-wave spectra of CrI_3, we show in Figs. 2(c)–2(e) the L dependence of spin waves at different in-plane wave vectors. Inspection of the figures reveals that the modes along the $[\frac{1}{2}, \frac{1}{2}, L]$ and $[0, 0, L]$ directions exhibit mutually opposite L dependence. Along the $[0, 0, L]$ direction, the spin-wave dispersion exhibits a minimum of 0.4 meV at $L = 3n$ ($n =$ integers) and a maximum of 2.1 meV at $L = 3n + \frac{3}{2}$ [Fig. 2(e)]. In contrast, the mode along the $[\frac{1}{2}, \frac{1}{2}, L]$ direction peaks at $L = 3n$ and has a minimum at $L = 3n + \frac{3}{2}$ [Fig. 2(c)], while spin waves along the $[\frac{1}{2}, 0, L]$ direction are featureless [Fig. 2(d)]. The overall spin-wave spectra at $L = 3$ and 4.5 are shown in Figs. 2(f) and 2(g), respectively. The opposite L dependence between the high- and low-energy spin waves requires finite FM interplane exchanges along the bonds that are tilted off the c axis.

To understand spin-wave spectra in Figs. 2 and 3, we consider a Heisenberg model with the DM interaction to account for the observed Dirac spin gap [23,24,30]. The Hamiltonian of the DM interaction, H_{DM}, can be written as $H_{\mathrm{DM}} = -\sum_{i<j}[\mathbf{A}_{ij}\cdot(\mathbf{S}_i \times \mathbf{S}_j)]$, where $\mathbf{S}_i$ and $\mathbf{S}_j$ are spins at sites i and j, respectively, and $\mathbf{A}_{ij}$ is the antisymmetric DM interaction between sites i and j [Figs. 1(a) and 1(c)]. The combined Heisenberg-DM (J-DM) Hamiltonian is $H_{\text{J-DM}} = \sum_{i<j}[J_{ij}\mathbf{S}_i\cdot\mathbf{S}_j + \mathbf{A}_{ij}\cdot\mathbf{S}_i\times\mathbf{S}_j] + \sum_j D_z(S_j^z)^2$, where J_{ij} is the magnetic exchange coupling of the $\mathbf{S}_i$ and $\mathbf{S}_j$, and D_z is the easy-axis anisotropy along the $z(c)$ axis [30]. As shown in Fig. 1(a), we define the in-plane NN, the next-nearest-neighbor (NNN), and the third NN interactions as J_1, J_2, and J_3, respectively. The c axis NN, the NNNs, and the third NN interactions are J_{c1}, J_{c2}/J_{c3}, and J_{c4}/J'_{c4}, respectively. For ideal honeycomb lattice materials where the NNN bond breaks the inversion symmetry [Fig. 1(c)], the DM vectors can have both in-plane ($\mathrm{DM}_{||}$) and out-of-plane ($\mathrm{DM}_{\perp}$) components, but the former will not contribute to the topological gap opening because of the threefold rotational symmetry of the honeycomb lattice [Fig. 1(d)]. As a result, only the DM term parallel to the c axis, i.e., the NNN DM interaction, will contribute to the opening of a spin gap in spin-wave spectra. Since bulk $\mathrm{CrI_3}$ orders ferromagnetically below a Curie temperature of $T_C \approx 61$ K with an ordered moment along the c axis [6], one can fit the spin-wave spectra and Dirac gap using the finite NNN H_{DM} ($\neq 0$), which may induce TRSB and topological spin excitations in the FM ordered state [30].

TABLE I. Magnetic exchange interaction strength (the negative value indicates the FM exchange) in the J-DM model, the electron correlation model, and the J-K-Γ model. Our estimated $\mathrm{DM}_{\perp} \approx 0.09$ meV is similar to that in Ref. [44].

Model	J-DM	J-J_{c4}	J-K-Γ
J_1 (meV)	−2.11	−2.11	−0.83
J_2 (meV)	−0.11	−0.11	−0.16
J_3 (meV)	0.10	0.10	0.08
J_{c1} (meV)	0.048	0.048	0.048
$J_{c2}(J_{c3})$ (meV)	−0.071	−0.071	−0.071
$J_{c4}(-J'_{c4})$ (meV)	0	−0.1	0
$\mathrm{DM}_{\perp}$ (meV)	0.09	0	0
K (meV)	0	0	−3.8
D_z (meV)	−0.123	−0.123	0
Γ (meV)	0	0	−0.082

The left panels of Figs. 2(c)–2(e) and 3(b) are the calculated spin-wave spectra with exchange parameters listed in Table I [30]. Given the nearly flat dispersion along the $[\frac{1}{2}, 0, L]$ direction shown in Fig. 2(d), we choose to set $J_{c2} = J_{c3}$ for the two interplane NNN exchanges of nearly identical bond lengths [Fig. 1(a)]. The best-fit parameters reveal that the NN interlayer magnetic interactions are AF with strong FM couplings along the NNN directions [Fig. 1(a)]. In addition, one must include a finite DM interaction A to account for the observed spin gap at the Dirac points [Figs. 3(a), 3(b), and 3(d)] [43]. To precisely determine the magnitude of A, we consider spin wave data at the Dirac point with a narrow c-axis integration range of $-0.5 \leq L \leq 0.5$ in Fig. 3(c). Figures 3(d) and 3(e) show calculated spin wave spectra taking into account the mosaic of the aligned single crystals of $\mathrm{CrI_3}$ without and with the NNN DM interactions, respectively. An energy cut through Dirac point reveals clearly that the calculated spectra with the NNN DM interaction fits the data better [Fig. 3(f)]. The best magnitude of A ($\mathrm{DM}_{\perp}$) is determined by the least squares method using the observed and calculated spin wave spectra [Fig. 3(g)]. Since the Dirac wave vector is along the zigzag bonds of the honeycomb lattice, the observation of a spin gap at the Dirac point indicates a symmetry-breaking field between the two Cr sublattices within the honeycomb lattice [Figs. 1(a) and 1(c)]. While the DM vectors may be oriented either along the c axis or perpendicular to it, only the c axis component can open the Dirac gap due to the threefold symmetry of the ideal honeycomb lattice. In addition, the magnitude of the gap is directly proportional to the c axis component of the ordered spins [44,45].

An alternative scenario to understand the observed spin gap at the Dirac point is through the Kitaev interaction that occurs across the nearest bond with bond-dependent anisotropic Ising-like exchange [Fig. 1(b)] [15], which also breaks the time-reversal symmetry and can inhabit nontrivial topological edge modes [19]. The Kitaev interaction Hamiltonian H_K is $H_K = \sum_{\langle ij\rangle\in\lambda\mu(\nu)}[KS_i^\nu S_j^\nu + \Gamma(S_i^\lambda S_j^\mu + S_i^\nu S_j^\lambda)]$, where ($\lambda$, μ, ν) are any permutation of (x, y, z), K is the strength of the Kitaev interaction, and Γ is the symmetric off-diagonal anisotropy that induces a spin gap at the Γ point [19,33]. The combined Heisenberg-Kitaev Hamiltonian, the so-called J-K-Γ Hamiltonian, is $H_{\text{J-K-}\Gamma} = \sum_{\langle ij\rangle\in\lambda\mu(\nu)}[J_{ij}\mathbf{S}_i\cdot\mathbf{S}_j + KS_i^\nu S_j^\nu + \Gamma(S_i^\lambda S_j^\mu + S_i^\nu S_j^\lambda)]$. By fitting the J-K-Γ Hamiltonian using the data shown in Fig. 3(a), we extract the exchange parameters shown in Table I, whose Kitaev term (−3.8 meV) is smaller than that of Ref. [33] (−5.6 meV) due to the smaller energy gap observed from better aligned samples. When FM ordered spins are oriented along the c axis [6], the spin Hamiltonian based on the Heisenberg-Kitaev exchanges can also reproduce the observed spin waves and energy gap at the Dirac point in $\mathrm{CrI_3}$ [33]. Therefore, one cannot determine whether the NNN DM or Kitaev model is responsible for the spin gap at Dirac points in the spin waves of $\mathrm{CrI_3}$ at zero field [33].

Finally, by using calculations beyond density functional theory (DFT), it was suggested that the observed Dirac spin gap arises from the electron correlations not considered in the usual DFT theory [34]. In this picture, the Dirac spin gap arises from the differences in c axis magnetic exchange pathways along the third NN J_{c4} and J'_{c4} [Fig. 1(a), and see Fig. 3 in Ref. [34]]. If this picture is correct, one would expect

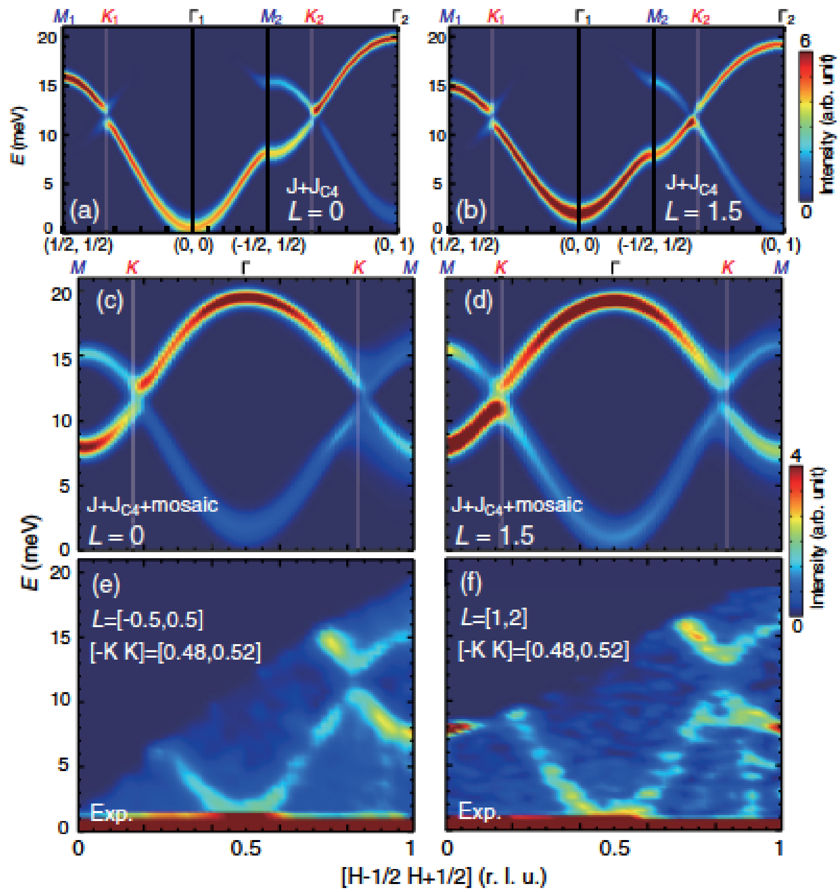

FIG. 4. The Heisenberg-J_{c4} (spin correlation) model simulation of CrI_3 spin wave spectra, here $J_{c4} = -J'_{c4} = -0.10$ meV. (a, b) In-plane spin excitation spectrum with $L = 0$ and 1.5, respectively. (c, d) Spin excitation spectra along (c) $[H - 1/2, H + 1/2, 0]$ and (d) $[H - 1/2, H + 1/2, 1.5]$ directions, respectively. The integration and mosaic effects are considered in the plot. (e, f) Experimental data corresponding to (c) and (d), respectively. The integration range of (c–f) are specified in (e) and (f).

that Dirac nodal lines, where acoustic and optical spin-wave bands cross, wind around the Dirac K point along the L direction [34]. Since both J_{c4} and J'_{c4} connect with Cr1 and do not break the CrI_3 sublattice symmetry, the electron correlation effects do not produce a true Dirac spin gap and only cause the Dirac crossing to shift sideways and induce nodal winding along the c axis. The spin-wave intensity winding around the Dirac point has been observed in the insulating easy-plane honeycomb quantum magnet $CoTiO_3$ without a Dirac spin gap and DM interaction, suggesting the nontrivial topology of the Dirac magnon wave functions [46–49].

Figures 4(a) and 4(b) show expected spin-wave spectra at $L = 0$ and 1.5, respectively, calculated using a Heisenberg Hamiltonian with magnetic exchange parameters specified in Table I. Near the Dirac points, we see spin gaplike features at K_1 and K_2 due to shifted acoustic-optical spin-wave touching points, and there is no true spin gap near the Dirac points. To compare with experimental observations, we calculate spin waves with the sample mosaic in Figures 4(c) and 4(d), which broaden spin waves but do not change their basic characters. Since experimental data at these L values show a clean spin gap at all wave vectors near the Dirac points [Figs. 4(e) and 4(f)]. We conclude that the observed Dirac spin gap cannot arise from the electron correlation effects as discussed in Ref. [34].

Since both the NNN DM and Kitaev models can describe spin waves of CrI_3 [33], it will be important to determine which microscopic model is correct. One way to separate these two scenarios is to do an inelastic neutron scattering experiment on CrI_3 with a magnetic field applied within the ab plane. The easy axis of spins in CrI_3 is parallel to the c axis, but a magnetic field of 3 T will turn the spin to the ab plane with almost zero out-of-plane components [6]. This change of the FM ordered moment direction will nullify the NNN DM term by making $\mathbf{A}_{ij}$ and $\mathbf{S}_i \times \mathbf{S}_j$ perpendicular to each other with vanishing $H_{\rm DM}$, and therefore close the NNN DM interaction-induced spin gap at the Dirac points [Fig. 1(d)]. This result is similar to the 2D kagome lattice ferromagnet Cu[1,3- benzenedicarboxylate (bdc)] [Cu(1,3-bdc)], where an out-of-plane magnetic field applied to align the in-plane FM ordered moments along the c axis is found to also induce a DM interaction-induced spin gap at the Dirac points [50,51]. In contrast, if the spin gap at the Dirac point is induced by the Kitaev exchange, its

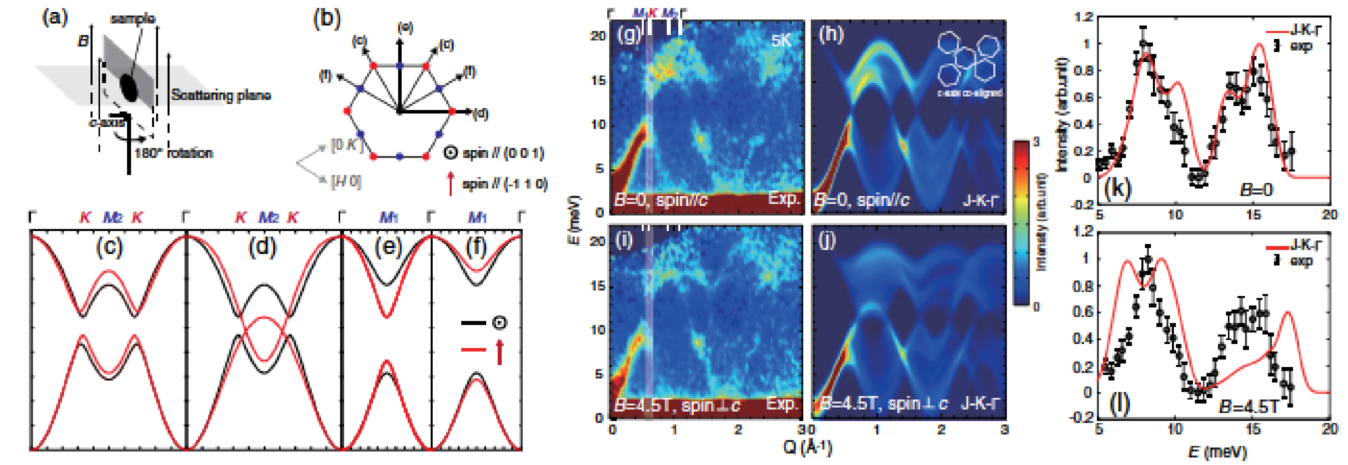

FIG. 5. The in-plane magnetic field effects on spin waves of c axis aligned CrI_3 single crystals shown in the inset of (h), and Heisenberg-Kitaev model fit of the spectra. (a) The experimental setup of inelastic neutron scattering experiments, where applied field is vertical and c axis of the crystals is in the light-shaded horizontal scattering plane. (b) The reciprocal lattice showing the scan direction in (c–f). The high symmetry points are shown with blue (M), red (K), and black (Γ) dots. (c–f) Spin wave dispersions of the Heisenberg-Kitaev model with in-plane (red) and out-of-plane (black) spin orientations. (g, i) Spin wave E-$\mathbf{Q}$ spectra of CrI_3 at 5 K in zero and 4.5 T in-plane fields, respectively. The high-symmetry points are marked on top. Here $\mathbf{Q}$ in the unit of Å^{1} indicates the wave vector s projection on the $[H, K]$ plane with $L = [-5, 5]$ integration. (h, j) Calculated E-$\mathbf{Q}$ spectra using the Heisenberg-Kitaev Hamiltonian at zero and 4.5 T field, respectively. (k, l) Comparison of the energy cuts between experiments (black dots) and calculations (red lines) using the Heisenberg-Kitaev Hamiltonian at Dirac point in 0 T and 4.5 T, respectively. The $\mathbf{Q}$ integration range of the energy cuts is 0.55–0.66 Å^{1} centered around the K point (= 0.608 Å^{1}), as shown in the long white shaded line in (g) and (i).

field dependence will be anisotropic and dependent on the relative angle of the polarized spin with respect to the in-plane lattice orientation [Figs. 5(a)–5(f)].

To test this idea, we perform inelastic neutron scattering experiments under in-plane magnetic fields on HYSPEC [41] with an incident neutron energy of $E_i = 27$ meV (Fig. 5) and on ARCS [42] with $E_i = 23$ meV (Fig. 6). Figure 5(a) shows the geometry of the experimental setups, where the applied magnetic fields are vertical in the honeycomb lattice plane. For HYSPEC experiments, we use c-axis aligned single crystals (~1 g) [see inset of Fig. 5(h)] and apply a field of 4.5 T, which is larger than the in-plane saturation field of 3 T [6] and sufficient to completely polarize the moment in the CrI_3 plane. As a function of increasing field, the spin gap at the Γ point (≈0.4 meV) [33] initially decreases to overcome the c-axis aligned moment but then increases because of the increasing Zeeman energy [43]. These results are consistent with the field dependence of the gap from either single-ion spin anisotropy or the off-diagonal Γ term in the Kitaev interaction [43].

Figures 5(g) and 5(i) show the spin-wave $\mathbf{Q}$-E spectra at zero and 4.5-T field, respectively. While the overall spin-wave intensity decreases at 4.5 T because of the rotation of the spin moment direction from the c axis to the CrI_3 plane, the spin gap near the Dirac point, marked by the white vertical line in Figs. 5(g) and 5(i), shows no obvious change. In the J-K-Γ model, the spin gap opens at the Dirac points because the NN Kitaev exchange interactions alternate between two different anisotropic bond-dependent terms along the zigzag bonds [19]. Since the Kitaev interaction Hamiltonian H_K is inherently sensitive to the spin orientations, spin-wave spectra of a J-K-Γ model will change drastically when the moment direction of the spins is rotated from the c axis to the in-plane direction by an externally applied magnetic field [Figs. 5(b)–5(f)]. Whereas a DM interaction-induced spin gap would close uniformly under an in-plane field to preserve the sixfold in-plane symmetry of the spin-wave dispersion, the Kitaev interaction-induced spin gaps will respond anisotropically depending on the relative angles between the wave vector and field direction. Furthermore, the field-induced changes in spin-wave spectra will not be limited around the Dirac points in the J-K-Γ model.

Figures 5(h) and 5(j) show calculated spin-wave $\mathbf{Q}$-E spectra using the J-K-Γ Hamiltonian with the c axis and in-plane moment, respectively. We use the exchange parameters that reproduce the zero field spectra identically with the Heisenberg-DM model shown in Fig. 3(b) [33]. While the zero field calculation agrees well with the data, the 4.5-T spin-wave spectra are clearly different from that of the calculation. The data points in Figs. 5(k) and 5(l) show energy-dependent spin waves across the Dirac point at 0 and 4.5 T, respectively. The solid lines are spin-wave calculations using the J-K-Γ Hamiltonian with the c axis and in-plane moments, confirming that the Heisenberg-

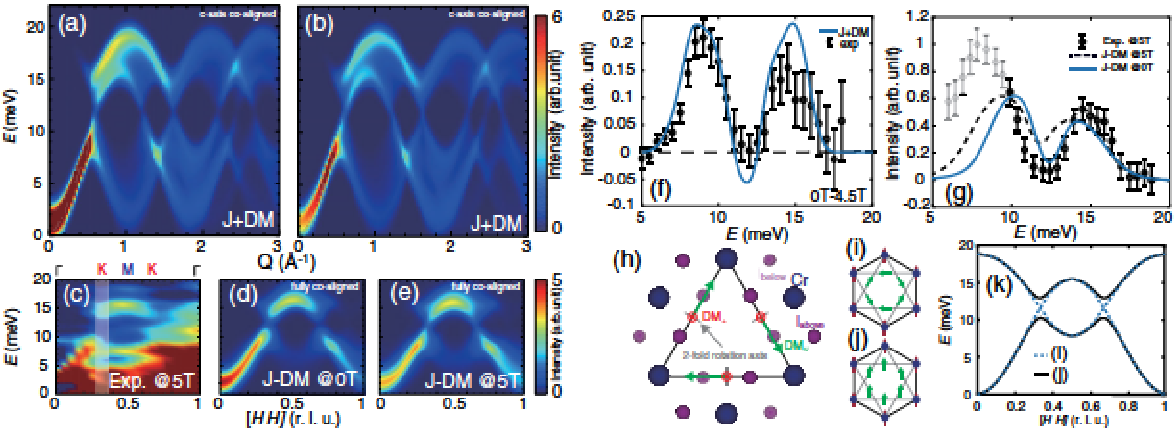

FIG. 6. The magnetic field effect on the Heisenberg-DM model. (a, b) Calculated E-$\mathbf{Q}$ spectra of c axis aligned CrI_3 using the Heisenberg-DM Hamiltonian with 0 and 4.5 T in-plane fields, respectively. (c) Spin waves of a fully co-aligned CrI_3 single crystals near the Dirac point along the $[H, H]$ direction with a 5 T in-plane magnetic field. (d, e) Heisenberg-DM model simulation with 0 and 5 T in-plane field, respectively. (f) The effect of a magnetic field on spin wave dispersion near Dirac point and its comparison with the Heisenberg-DM calculations. (g) Constant-Q cut at the Dirac point ($[H, H] = (0.3, 0.37)$) on the experimental data and Monte Carlo simulations. The experimental data has a constant background subtracted. The gray dots show intensity increasing due to higher instrumental background. (h) Schematics of the in-plane DM interaction of a triangular sublattice in one Cr hexagon. The in-plane component of the DM interaction ($DM_{\|}$) is perpendicular to the two-fold rotation axis between the two NN Cr ions according to the Moriya s rule. (i) In-plane DM interactions respecting the three-fold symmetry of the lattice. (j) An example of in-plane DM interactions breaking the three-fold symmetry of the lattice. (k) The calculation of spin wave dispersion with in-plane spins and in-plane DM interactions shown in red dashed lines (i) and black solid lines (j). Here $DM_{\|} = 0.17$ meV.

Kitaev Hamiltonian clearly fails to describe the magnetic field effect on spin waves.

Figures 6(a) and 6(b) show calculated spin-wave $\mathbf{Q}$-E spectra using the Heisenberg-DM Hamiltonian with the c axis and in-plane moment, respectively. Compared with the J-K-Γ Hamiltonian in Figs. 5(h) and 5(j), the Heisenberg-DM Hamiltonian obviously agrees much better with the experimental data in Figs. 5(g) and 5(i). Figure 6(c) shows the $\mathbf{Q}$-E dependence of spin waves near the Dirac point with an in-plane applied field of 5.0 T at 5 K, obtained on coaligned single crystals of CrI_3 on ARCS. Figures 6(d) and 6(e) are the corresponding spin-wave spectra calculated using the Heisenberg-DM Hamiltonian. The data points in Fig. 6(f) show the magnetic field difference plot obtained from Figs. 5(k) and 5(l). It is clear that the solid line calculated from the Heisenberg-DM Hamiltonian can approximately describe the data but with a small deviation near the Dirac point [Figs. 6(f) and 6(g)].

From the above discussions, we see that the J-K-Γ Hamiltonian clearly cannot describe the observed magnetic field dependence of spin waves in CrI_3. While the simple NNN Heisenberg-DM Hamiltonian can describe the overall spectra and its magnetic field dependence, it may have difficulty in describing the magnetic field dependence of the Dirac spin gap. Since the loss of translational symmetry between the two Cr sublattice spins of an ideal honeycomb lattice can open a spin gap at the Dirac points, it is important to determine other possible origins for the observed Dirac gap.

III. DISCUSSION

In previous work [1,35–39], A-type AF order of CrI_3 was found to be associated with the monoclinic structural phase either near the surface of the bulk or in thin-layer form (for example, the bilayer of CrI_3). However, it is unclear why the AF order in bilayer CrI_3 has monoclinic crystal structure, which appears in the paramagnetic phase above T_C of bulk CrI_3 [1,35,36]. Using the NN AF and NNN FM interlayer coupling in the rhombohedral FM phase (Figs. 1 and 2), we estimate that the interlayer stacking is still FM in the bilayer limit [43], thus ruling out

TABLE II. Estimated magnetic bonding energies associated with each Cr^{3+} atom in various crystal structure and exchange couplings [43]. Rhom and mono indicate rhombohedral and monoclinic lattice structures, respectively. In the hypothetical mono-bulk and mono-bilayer cases, the NN and NNN magnetic exchange couplings are assumed to be the same as those of the rhom-bulk and rhom-bilayer, revealing that the FM rhombohedral lattice structure has lower magnetic bonding energy.

Structures	J_{c1} (meV)	J_{c2} (meV)	Energy (meV)
Rhom-bulk, FM	0.048	−0.071	−1.33
Rhom-bilayer, FM	0.048	−0.071	−0.66
Mono-bulk, FM	0.048	−0.071	−0.21
Mono-bilayer, FM	0.048	−0.071	−0.10
Mono-bulk, AF	0.037	0	−0.33
Mono-bilayer, AF	0.037	0	−0.17

rhombohedral AF bilayer structure. If we change the crystal structure to monoclinic but maintain the NN and NNN c-axis coupling in bulk CrI_3, the magnetic bonding energies are higher than that of the rhombohedral lattice structure. From Raman scattering of bilayer CrI_3, the sum of the interlayer AF coupling in monoclinic structure was found to be about 0.11 meV [36]. Assuming that the NNN magnetic exchange is negligible, we estimate that the NN magnetic exchange in the monoclinic bilayer is $J_{c1} = 0.037$ meV [43]. Table II summarizes the total magnetic bonding energy for one Cr^{3+} atom in different lattice and magnetic structures [43]. We find that the FM bilayer rhombohedral structure should be more favorable than the AF bilayer monoclinic structure, contrary to the observation. Since Raman experiments can only deduce total magnetic exchange along the c axis, we are unable to determine the actual NN and NNN magnetic exchange couplings in the monoclinic structure. Nevertheless, the observed AF order in the monoclinic bilayer suggests that such a phase has lower ground-state energy compared with that of the FM rhombohedral structure in bulk or bilayer CrI_3. As the hydrostatic pressure applied on the AF bilayer CrI_3 can reduce the interlayer spacing and reintroduce the rhombohedral FM state [38], we expect that the monoclinic bilayer CrI_3 should have a larger c-axis AF exchange and lattice parameter compared with that of the rhombohedral bilayer. This case is also consistent with a reduced c-axis lattice constant below T_C in bulk CrI_3 [6] and recent simulations of transport measurements suggesting that the layers may expand along the c axis to minimize interaction energy and stabilize a different magnetic coupling [52,53]. We note that the collinear AF order in iron pnictides also expands the lattice parameter along the AF ordering direction [54,55]. While the NNN interlayer exchange couplings of bulk CrI_3 ultimately determines its FM ground state, the AF interlayer coupling prevails in the monoclinic bilayer CrI_3 [43]. These results suggest that the monoclinic-to-rhombohedral structural phase transition in CrI_3 is driven by reducing the interlayer magnetic exchange energy.

Although our data rule out a pure Kitaev interaction and electron correlations as the microscopic origins of the observed Dirac spin gap, there may be other interactions in addition to the NNN DM that contribute to the Dirac spin gap. We consider several possibilities. First, reducing the bulk structural symmetry from rhombohedral to monoclinic, by itself, will not open a spin gap at the Dirac point because such a structural phase transition does not change the inversion symmetry of the Cr honeycomb sublattice. If additional structural deformations are present due to, for instance, thermal effects, the inversion center between the first NNs would be removed, which, incidentally, would allow DM interactions to exist at that level. Nevertheless, we show in the Supplemental Material [43] that the inclusion of DM at the first NNs does not open a gap at the Dirac point. We also consider a Heisenberg model with both the NNN DM and Kitaev interaction [43]. By using a Heisenberg-DM Hamiltonian with different Kitaev interaction strengths that fits spin-wave spectra at 0 T, we can compare the expected and observed spin waves under a 4.5-T field and in-plane spin. The result indicates that the Kitaev term should be near zero in order to get the best fit to the 4.5-T spin-wave spectra [43].

Alternatively, magnon-magnon interactions may potentially affect H_{DM}, which can result in a gap at the Dirac point. When higher-order Holstein-Primakoff transformations are considered in the description of the spin interactions in CrI_3, three-operator products arise which may contribute to the gap [43]. However, since magnon-magnon interactions in most magnetic materials are weakly energy and wave vector dependent, and typically occur at energies above the single magnon scattering, they are unlikely to give rise to the observed spin gap at the Dirac points.

Finally, we envision two mechanisms that may allow the spin gap at the Dirac point to remain open under an in-plane spin-polarizing field: The first is the sublattice symmetry breaking, and the second is the threefold rotational symmetry breaking of the ideal honeycomb lattice of CrI_3.

We first discuss the possible sublattice symmetry breaking of an ideal honeycomb lattice. From spin-wave spectra in Figs. 2 and 3, we know that the two Cr^{3+} ions of different sublattices within the honeycomb unit cell interact not only via the intralayer NN interaction J_1 but also the interlayer NN J_{c1}, which is AF and directly along the c axis [Fig. 1(a)]. Whereas both bonds are bisected by the structural inversion centers, respectively, the interlayer AF exchange coupling J_{c1} will favor a breaking of the inversion symmetry between the two Cr sublattice spins. As a result, if the two Cr^{3+} ions within a unit cell have spins of unequal moments (due to environmental defects such as Cr and/or I vacancy) [56], an energy gap will appear at the Dirac points without significantly affecting spin waves at other wave vectors.

It is well known that the interlayer magnetic order in CrI_3 switches from AF to FM as the number of stacked vdW layers increases from the bilayer to the bulk, accompanied by a structural transition from monoclinic to rhombohedral stacking along the c axis [57–62]. In addition, a small (< 3 T) in-plane magnetic field can easily transform AF ordered multilayer CrI_3 into a ferromagnet [63]. Even in the bulk samples, the surface layers are reported to have AF monoclinic structure that can be tuned by a c-axis aligned magnetic field of a few Tesla [39]. While these results indicate minor energy differences in rhombohedral and monoclinic structures of CrI_3, they suggest that the Cr honeycomb lattice may have subtle NN inversion symmetry-breaking structural distortions that are responsible for the observed Dirac spin gap [56].

We next consider the field-induced breaking of the threefold symmetry of the in-plane DM vectors. Since the NNN DM interaction must involve the iodine atoms, the mirror symmetry of the simple honeycomb lattice is lost, with only the twofold rotation axis remaining [43]. As a result, the DM vector is not constrained to be out of plane and can have in-plane projections. This argument holds as long as the DM vector is perpendicular to the twofold rotation axis according to Moriya's rule [Fig. 6(h)]. In the case where no magnetic field is applied, the spins are aligned along the c axis, and only the DM vector component parallel to this direction can open the Dirac gap. In the situation where an in-plane applied magnetic field is strong enough to rotate the c axis aligned spins into the CrI_3 plane, the threefold symmetry of the in-plane DM vectors will cancel out when determining the spin-wave energy at the K point, thus yielding no contribution to the Dirac gap [Figs. 6(i) and 6(j)]. However, if the in-plane DM vector breaking the threefold symmetry is induced by the applied field, then it will contribute to opening a Dirac gap [Fig. 6(k)]. This process will require a significant field-induced symmetry breaking of the in-plane DM whose energy scale should be similar to the out-of-plane DM terms (~0.17 meV). While a c axis aligned magnetic field of a few Tesla is known to break the lattice symmetry of CrI_3 [39], there is currently no direct experimental proof that an in-plane magnetic field of a few Tesla would break the threefold symmetry of the crystalline lattice in CrI_3. Nevertheless, we could estimate a band gap of ~1.1 meV using the parameters extracted from our data, which underestimates the gap value obtained from the experiments due to the mosaicity effect [43]. This conjecture suggests that the Cr lattice, as well as its halide sublattice, contributes to the topological spin features observed in CrI_3.

IV. CONCLUSIONS

In summary, we used inelastic neutron scattering to study the impact of an in-plane magnetic field on spin waves of CrI_3. At zero field, we completely determined the magnetic exchange couplings along the c axis by carefully measuring c-axis spin-wave dispersions at different in-plane wave vectors. We find that the NN c-axis magnetic exchange coupling is AF and the NNN magnetic exchange couplings are FM. These results thus indicate coexisting AF and FM exchange interactions between the hexagonal layers of CrI_3. We also confirmed the presence of a spin gap at the Dirac points at zero field and found that an in-plane magnetic field that can rotate the moment from the c axis to the CrI_3 plane also modifies the spin-wave spectra and spin gap at Dirac points. These results can conclusively rule out the J-K-Γ Hamiltonian and electron correlations as origins of the Dirac spin gap. While the field dependence of the Dirac spin gap may not be completely understood within the NNN Heisenberg-DM Hamiltonian, the results suggest the presence of a local sublattice or threefold rotational symmetry breaking of the ideal honeycomb lattice in CrI_3. Our results therefore firmly establish the microscopic spin Hamiltonian in CrI_3 and provide a new understanding of topology-driven spin excitations in 2D vdW magnets.

ACKNOWLEDGMENTS

We are grateful to Franz G. Utermohlen, Nandini Trivedi, Adam Tsen, Zurab Guguchia, Liuyan Zhao, and Rui He for helpful discussions. The neutron scattering and sample growth work at Rice is supported by U.S. NSF-DMR-1700081 and by the Robert A. Welch Foundation under Grant No. C-1839 (P. D.). The work of J. H. C. was supported by the National Research Foundation (NRF) of Korea (Grants No. 2020R1A5A1016518 and No. 2020K1A3A7A09077712). E. J. G. S. acknowledges computational resources through the CIRRUS Tier-2 HPC Service (ec131 CirrusProject) at EPCC funded by the University of Edinburgh and EPSRC (EP/P020267/1); and ARCHER UK National Supercomputing Service via Project d429. E. J. G. S. acknowledges the EPSRC Early Career Fellowship (EP/T021578/1) and the University of Edinburgh for funding support. A portion of this research used resources at the Spallation Neutron Source, a DOE Office of Science User Facility operated by the Oak Ridge National Laboratory.

[1] B. Huang *et al.*, *Layer-Dependent Ferromagnetism in a van der Waals Crystal down to the Monolayer Limit*, Nature (London) **546**, 270 (2017).

[2] C. Gong *et al.*, *Discovery of Intrinsic Ferromagnetism in Two-Dimensional van der Waals Crystals*, Nature (London) **546**, 265 (2017).

[3] Z. Zhang, J. Shang, C. Jiang, A. Rasmita, W. Gao, and T. Yu, *Direct Photoluminescence Probing of Ferromagnetism in Monolayer Two-Dimensional* $CrBr_3$, Nano Lett. **19**, 3138 (2019).

[4] K. S. Burch, D. Mandrus, and J.-G. Park, *Magnetism in Two-Dimensional van der Waals Materials*, Nature (London) **563**, 47 (2018).

[5] M. Gibertini, M. Koperski, A. F. Morpurgo, and K. S. Novoselov, *Magnetic 2D Materials and Heterostructures*, Nat. Nanotechnol. **14**, 408 (2019).

[6] M. A. McGuire, H. Dixit, V. R. Cooper, and B. C. Sales, *Coupling of Crystal Structure and Magnetism in the Layered, Ferromagnetic Insulator* CrI_3, Chem. Mater. **27**, 612 (2015).

[7] M. A. Mcgurie, *Crystal and Magnetic Structures in Layered, Transition Metal Dihalides and Trihalides*, Crystal **7**, 121 (2017).

[8] J. Kanamori, *Superexchange Interaction and Symmetry Properties of Electron Orbitals*, J. Phys. Chem. Solids **10**, 87 (1959).

[9] D.-H. Kim, K. Kim, K.-T. Ko, J. H. Seo, J. S. Kim, T.-H. Jang, Y. Kim, J.-Y. Kim, S.-W. Cheong, and J.-H. Park, *Giant Magnetic Anisotropy Induced by Ligand LS Coupling in Layered Cr Compounds*, Phys. Rev. Lett. **122**, 207201 (2019).

[10] A. T. Costa, D. L. R. Santos, N. M. R. Peres, and J. Fernández-Rossier, *Topological Magnons in* $\mathrm{CrI_3}$ *Monolayers: An Itinerant Fermion Description*, 2D Mater. **7**, 045031 (2020).

[11] N. D. Mermin and H. Wagner, *Absence of Ferromagnetism or Antiferromagnetism in One- or Two-Dimensional Isotropic Heisenberg Models*, Phys. Rev. Lett. **17**, 1133 (1966).

[12] A. Kartsev, M. Augustin, R. F. L. Evans, K. S. Novoselov, and E. J. G. Santos, *Biquadratic Exchange Interactions in Two-Dimensional Magnets*, npj Comput. Mater. **6**, 150 (2020).

[13] M. Augustin, S. Jenkins, R. F. L. Evans, K. S. Novoselov, and E. J. G. Santos, *Properties and Dynamics of Meron Topological Spin Textures in the Two-Dimensional Magnet* $\mathrm{CrCl_3}$, Nat. Commun. **12**, 185 (2021).

[14] D. A. Wahab *et al.*, *Quantum Rescaling, Domain Metastability, and Hybrid Domain-Walls in 2D* $\mathrm{CrI_3}$ *Magnets*, Adv. Mater. **33**, 2004138 (2021).

[15] A. Y. Kitaev, *Anyons in an Exactly Solved Model and Beyond*, Ann. Phys. (Amsterdam) **321**, 2 (2006).

[16] G. Jackeli and G. Khaliullin, *Mott Insulators in the Strong Spin-Orbit Coupling Limit: From Heisenberg to a Quantum Compass and Kitaev Models*, Phys. Rev. Lett. **102**, 017205 (2009).

[17] H. Takagi, T. Takayama, G. Jackeli, G. Khaliullin, and S. E. Nagler, *Concept and Realization of Kitaev Quantum Spin Liquids*, Nat. Rev. Phys. **1**, 264 (2019).

[18] C. Xu, J. Feng, H. Xiang, and L. Bellaiche, *Interplay between Kitaev Interaction and Single Ion Anisotropy in Ferromagnetic* $\mathrm{CrI_3}$ *and* $\mathrm{CrGeTe_3}$ *Monolayers*, npj Comput. Mater. **4**, 57 (2018).

[19] I. Lee, F. G. Utermohlen, D. Weber, K. Hwang, C. Zhang, J. van Tol, J. E. Goldberger, N. Trivedi, and P. C. Hammel, *Fundamental Spin Interactions Underlying the Magnetic Anisotropy in the Kitaev Ferromagnet* $\mathrm{CrI_3}$, Phys. Rev. Lett. **124**, 017201 (2020).

[20] P. P. Stavropoulos, X. Liu, and H.-Y. Kee, *Magnetic Anisotropy in Spin-*$3/2$ *with Heavy Ligand in Honeycomb Mott Insulators: Application to* $\mathrm{CrI_3}$, Phys. Rev. Research **3**, 013216 (2021).

[21] D. G. Joshi, *Topological Excitations in the Ferromagnetic Kitaev-Heisenberg Model*, Phys. Rev. B **98**, 060405(R) (2018).

[22] E. Aguilera, R. Jaeschke-Ubiergo, N. Vidal-Silva, L. E. F. F. Torres, and A. S. Nunez, *Topological Magnonics in the Two-Dimensional van der Waals Magnet* $\mathrm{CrI_3}$, Phys. Rev. B **102**, 024409 (2020).

[23] S. A. Owerre, *A First Theoretical Realization of Honeycomb Topological Magnon Insulator*, J. Phys. Condens. Matter **28**, 386001 (2016).

[24] S. K. Kim, H. Ochoa, R. Zarzuela, and Y. Tserkovnyak, *Realization of the Haldane-Kane-Mele Model in a System of Localized Spins*, Phys. Rev. Lett. **117**, 227201 (2016).

[25] A. H. C. Neto, F. Guinea, N. M. R. Peres, K. S. Novoselov, and A. K. Geim, *The Electronic Properties of Graphene*, Rev. Mod. Phys. **81**, 109 (2009).

[26] F. D. M. Haldane, *Model for a Quantum Hall Effect without Landau Levels: Condensed-Matter Realization of the "Parity Anomaly"*, Phys. Rev. Lett. **61**, 2015 (1988).

[27] A. V. Chumak, V. I. Vasyuchka, A. A. Serga, and B. Hillebrands, *Magnon Spintronics*, Nat. Phys. **11**, 453 (2015).

[28] A. L. Chernyshev and P. A. Maksimov, *Damped Topological Magnons in the Kagome-Lattice Ferromagnets*, Phys. Rev. Lett. **117**, 187203 (2016).

[29] X. S. Wang, Y. Su, and X. R. Wang, *Topologically Protected Unidirectional Edge Spin Waves and Beam Splitter*, Phys. Rev. B **95**, 014435 (2017).

[30] L. Chen, J.-H. Chung, B. Gao, T. Chen, M. B. Stone, A. I. Kolesnikov, Q. Huang, and P. Dai, *Topological Spin Excitations in Honeycomb Ferromagnet* $\mathrm{CrI_3}$, Phys. Rev. X **8**, 041028 (2018).

[31] I. Dzyaloshinskii, *A Thermodynamic Theory of "Weak" Ferromagnetism of Antiferromagnetics*, J. Phys. Chem. Solids **4**, 241 (1958).

[32] T. Moriya, *Anisotropic Superexchange Interaction and Weak Ferromagnetism*, Phys. Rev. **120**, 91 (1960).

[33] L. Chen *et al.*, *Magnetic Anisotropy in Ferromagnetic* $\mathrm{CrI_3}$, Phys. Rev. B **101**, 134418 (2020).

[34] L. Ke and M. I. Katsnelson, *Electron Correlation Effects on Exchange Interactions and Spin Excitations in 2D van der Waals Materials*, npj Comput. Mater. **7**, 4 (2021).

[35] X.-X. Zhang, L. Li, D. Weber, J. Goldberger, K. F. Mak, and J. Shan, *Gate-Tunable Spin Waves in Antiferromagnetic Atomic Bilayers*, Nat. Mater. **19**, 838 (2020).

[36] J. Cenker *et al.*, *Direct Observation of Two-Dimensional Magnons in Atomically Thin* $\mathrm{CrI_3}$, Nat. Phys. **17**, 20 (2021).

[37] T. Li *et al.*, *Pressure-Controlled Interlayer Magnetism in Atomically Thin* $\mathrm{CrI_3}$, Nat. Mater. **18**, 1303 (2019).

[38] T. Song *et al.*, *Switching 2D Magnetic States via Pressure Tuning of Layer Stacking*, Nat. Mater. **18**, 1298 (2019).

[39] S. Li *et al.*, *Magnetic-Field-Induced Quantum Phase Transitions in a van der Waals Magnet*, Phys. Rev. X **10**, 011075 (2020).

[40] G. E. Granroth, A. I. Kolesnikov, T. E. Sherline, J. P. Clancy, K. A. Ross, J. P. C. Ruff, B. D. Gaulin, and S. E. Nagler, *SEQUOIA: A Newly Operating Chopper Spectrometer at the SNS*, J. Phys. Conf. Ser. **251**, 012058 (2010).

[41] B. Winn *et al.*, *Recent Progress on HYSPEC, and Its Polarization Analysis Capabilities*, EPJ Web Conf. **83**, 03017 (2015).

[42] D. L. Abernathy, M. B. Stone, M. J. Loguillo, M. S. Lucas, O. Delaire, X. Tang, J. Y. Y. Lin, and B. Fultz, *Design and Operation of the Wide Angular-Range Chopper Spectrometer ARCS at the Spallation Neutron Source*, Rev. Sci. Instrum. **83**, 015114 (2012).

[43] See Supplemental Material at http://link.aps.org/supplemental/10.1103/PhysRevX.000.000000 for additional data and analysis.

[44] Y. O. Kvashnin, A. Bergman, A. I. Lichtenstein, and M. I. Katsnelson, *Relativistic Exchange Interactions in* $Cr\,X_3$ $(X = \mathrm{Cl},\ Br,\ I)$ *Monolayers*, Phys. Rev. B **102**, 115162 (2020).

[45] A. Mook, K. Plekhanov, J. Klinovaja, and D. Loss, *Interaction-Stabilized Topological Magnon Insulator in Ferromagnets*, Phys. Rev. X **11**, 021061 (2021).

[46] S. S. Pershoguba, S. Banerjee, J. C. Lashley, J. Park, H. Ågren, G. Aeppli, and A. V. Balatsky, *Dirac Magnons in Honeycomb Ferromagnets*, Phys. Rev. X **8**, 011010 (2018).

[47] P. A. McClarty and J. G. Rau, *Non-Hermitian Topology of Spontaneous Magnon Decay*, Phys. Rev. B **100**, 100405(R) (2019).

[48] B. Yuan, I. Khait, G.-J. Shu, F. C. Chou, M. B. Stone, J. P. Clancy, A. Paramekanti, and Y.-J. Kim, *Dirac Magnons in a Honeycomb Lattice Quantum XY Magnet* $CoTiO_3$, Phys. Rev. X **10**, 011062 (2020).

[49] M. Elliot, P. A. McClarty, D. Prabhakaran, R. D. Johnson, H. C. Walker, P. Manuel, and R. Coldea, *Visualization of Isospin Momentum Texture of Dirac Magnons and Excitons in a Honeycomb Quantum Magnet*, arXiv:2007.04199v1.

[50] R. Chisnell, J. S. Helton, D. E. Freedman, D. K. Singh, R. I. Bewley, D. G. Nocera, and Y. S. Lee, *Topological Magnon Bands in a Kagome Lattice Ferromagnet*, Phys. Rev. Lett. **115**, 147201 (2015).

[51] R. Chisnell, J. S. Helton, D. E. Freedman, D. K. Singh, F. Demmel, C. Stock, D. G. Nocera, and Y. S. Lee, *Magnetic Transitions in the Topological Magnon Insulator Cu(1,3-bdc)*, Phys. Rev. B **93**, 214403 (2016).

[52] Z. Wang, I. Gutiérrez-Lezama, N. Ubrig, M. Kroner, M. Gibertini, T. Taniguchi, K. Watanabe, A. Imamolu, E. Giannini, and A. F. Morpurgo, *Very Large Tunneling Magnetoresistance in Layered Magnetic Semiconductor* CrI_3, Nat. Commun. **9**, 2516 (2018).

[53] F. Cantos-Prieto, A. Falin, M. Alliati, D. Qian, R. Zhang, T. Tao, M. R. Barnett, E. J. G. Santos, L. H. Li, and E. Navarro-Moratalla, *Layer-Dependent Mechanical Properties and Enhanced Plasticity in the van der Waals Chromium Trihalide Magnets*, Nano Lett. **21**, 3379 (2021).

[54] C. de la Cruz *et al.*, *Magnetic Order Close to Superconductivity in the Iron-Based Layered* $LaO_{1-x}F_xFeAs$ *Systems*, Nature (London) **453**, 899 (2008).

[55] J. Zhao, W. Ratcliff II, J. W. Lynn, G. F. Chen, J. L. Luo, N. L. Wang, J. Hu, and P. Dai, *Spin and Lattice Structures of Single-Crystalline* $SrFe_2As_2$, Phys. Rev. B **78**, 140504(R) (2008).

[56] J. Meseguer-Sanchez, D. A. Wahab, H. Luetkens, G. Taniashvili, E. Navarro-Moratalla, Z. Guguchia, and E. J. G. Santos, *Thermal Disorder Driven Magnetic Phases in van der Waals Magnet* CrI_3, arXiv:2010.04544.

[57] P. Jiang, C. Wang, D. Chen, Z. Zhong, Z. Yuan, Z.-Y. Lu, and W. Ji, *Stacking Tunable Interlayer Magnetism in Bilayer* CrI_3, Phys. Rev. B **99**, 144401 (2019).

[58] J. Shang, X. Tang, X. Tan, A. Du, T. Liao, S. C. Smith, Y. Gu, C. Li, and L. Kou, *Stacking-Dependent Interlayer Magnetic Coupling in 2D* $CrI_3/CrGeTe_3$ *Nanostructures for Spintronics*, ACS Appl. Nano Mater. **3**, 1282 (2020).

[59] S. W. Jang, M. Y. Jeong, H. Yoon, S. Ryee, and M. J. Han, *Microscopic Understanding of Magnetic Interactions in Bilayer* CrI_3, Phys. Rev. Mater. **3**, 031001(R) (2019).

[60] B. Niu *et al.*, *Coexistence of Magnetic Orders in Two-Dimensional Magnet* CrI_3, Nano Lett. **20**, 553 (2020).

[61] B. Huang, J. Cenker, X. Zhang, E. L. Ray, T. Song, T. Taniguchi, K. Watanabe, M. A. McGuire, D. Xiao, and X. Xu, *Tuning Inelastic Light Scattering via Symmetry Control in the Two-Dimensional Magnet* CrI_3, Nat. Nanotechnol. **15**, 212 (2020).

[62] Z. Sun *et al.*, *Giant Nonreciprocal Second-Harmonic Generation from Antiferromagnetic Bilayer* CrI_3, Nature (London) **572**, 497 (2019).

[63] A. McCreary *et al.*, *Distinct Magneto-Raman Signatures of Spin-Flip Phase Transitions in* CrI_3, Nat. Commun. **11**, 3879 (2020).